ACCOUNTS of chemical research

pubs.acs.org/accounts

Article

Misfit Layered Compounds: Insights into Chemical, Kinetic, and Thermodynamic Stability of Nanophases

Azat Khadiev,[†] M. B. Sreedhara,*[,†] Simon Hettler, Dmitri Novikov, Raul Arenal, and Reshef Tenne*

Cite This: *Acc. Chem. Res.* 2024, 57, 3243−3253

Read Online

ACCESS | Metrics & More | Article Recommendations | Supporting Information

CONSPECTUS: Compounds with layered structures (2D-materials), like transition metal-dichalcogenides (e.g., MoS_2), attracted a great deal of interest in the scientific community in recent years. This interest can be attributed to their unique lamellar structure, which induces large anisotropy in their physicochemical properties. Furthermore, owing to the weak van der Waals interaction between the layers, they can be cleaved along the *a*−*b* plane, which allows fabricating single layers with physical properties entirely different from the bulk material. Moreover, stacking layers of different 2D-materials on top of each other has led to a wealth of new observations, for instance, by twisting two layers with respect to each other and producing Moiré lattice. Another outstanding property of inorganic layer compounds is their tendency to form nanotubes, reported first (for WS_2) many years ago and subsequently from many other layered compounds.

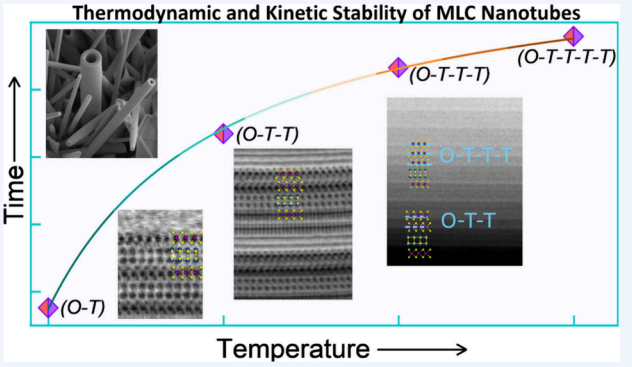

Among the 2D-materials, misfit layer compounds make a special class with an incommensurate and nonstoichiometric lattice made of an alternating layer with rocksalt structure, like LaS (*O*) and a layer with hexagonal structure, like TaS_2 (*T*). The lack of lattice commensuration between the two slabs leads to a built-in strain, which can be relaxed via bending. Consequently, nanotubes have been produced from numerous MLC compounds over the past decade and their structure was elucidated.

Owing to their large surface area, nanostructures are generally metastable and tend to recrystallize into microscopic crystallites via different mechanisms, like Ostwald ripening, or chemically decompose and then recrystallize. The stability of nanostructures at elevated temperatures has been investigated quite scarcely so far. In this perspective, electron microscopy as well as synchrotron-based X-ray absorption and reflection techniques were used to elucidate the chemical selectivity and decomposition routes of rare-earth based MLC nanotubes prepared at elevated temperatures (800−1200 °C).

As for the chemical selectivity, entropic effects are expected to dictate the random distribution of the chalcogen atoms on the anion sites of the MLC nanotubes at elevated temperatures. Nonetheless, the sulfur atoms were found to bind exclusively to the rare-earth atom (Ln = La, Sm) of the rocksalt slab and the selenium to the tantalum of the hexagonal TX_2 slab. This uncommon selectivity was not found in other kinds of nanotubes like $WSe_{2x}S_{2(1-x)}$. In other series of experiments, the lack of utter symmetry in the multiwall nanotubes leads to exclusions of certain X-ray (0*kl*) reflections, which was used to distinguish them from the bulk crystallites. The transformation of Ln-based MLC nanotubes into microscopic flakes was followed as a function of the synthesis temperature (800−1200 °C) and the synthesis time (1−96 h). Furthermore, sequential high-temperature transformations of the (*O*-*T*) lattice into (*O*-*T*-*T*) and finally (*O*-*T*-*T*-*T*) phases via deintercalation of the LnS slab was observed. This autocatalytic process is reminiscent of the deintercalation of alkali atoms from different layered structure materials. Annealing at higher temperatures and for longer periods of time eventually leads to the decomposition of the ternary MLC into binary metal-sulfide phases, as well as partial oxidation of the product. This study sheds light on the complex mechanism of high-temperature chemical stability of the nanostructures.

KEY REFERENCES

- Sreedhara, M. B.; Khadiev, A.; Zheng, K.; Hettler, S.; Serra, M.; Castelli, I. E.; Arenal, R.; Novikov, D.; Tenne, R. Nanotubes from Lanthanide-Based Misfit-Layered Compounds: Understanding the Growth, Thermodynamic, and Kinetic Stability Limits. *Chem. Mater.* **2024**, *36* (9), 4736−4749.[1] Demonstrates a synchrotron-based X-ray diffraction approach to study the degradation mechanism of nanophases in bulk powder and gives insights into the degradation mechanism of LnS-TaS_2 MLC nanotubes at high temperatures.

Received: June 29, 2024
Revised: October 19, 2024
Accepted: October 21, 2024
Published: November 4, 2024

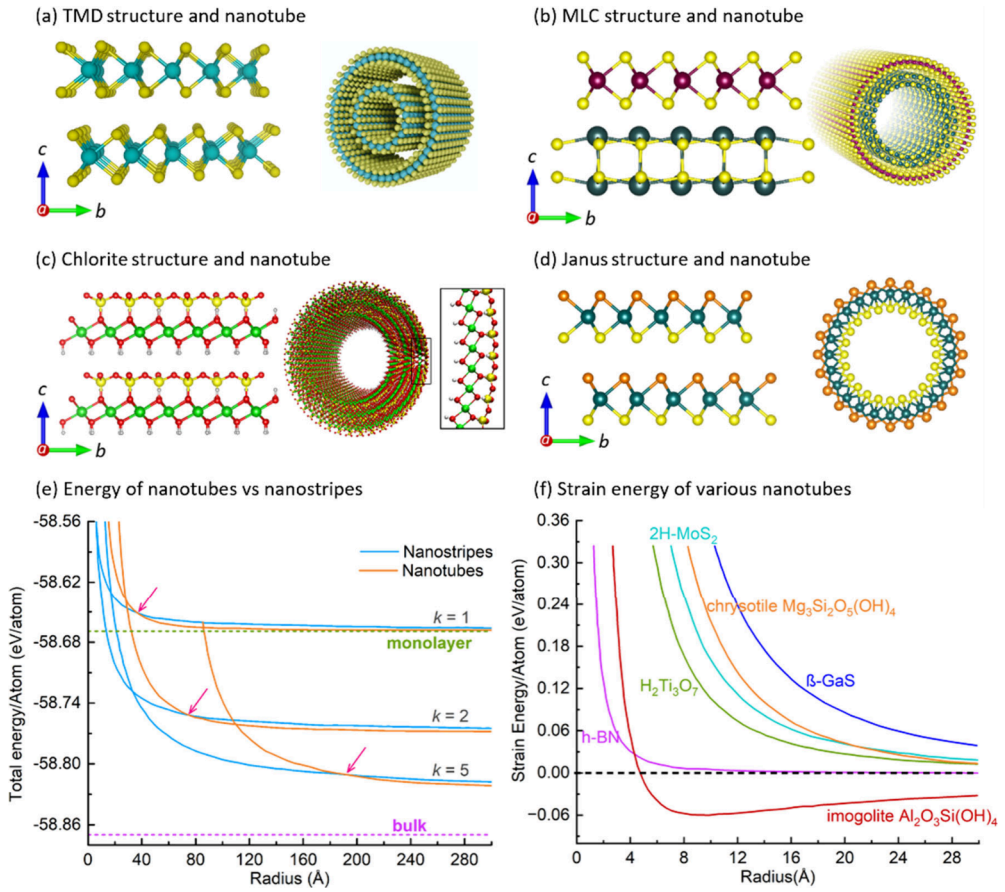

Figure 1. Schematic rendering of the various layered materials (a–d) and their corresponding nanotubes with different strain energy of folding. (a) Structure of TMDCs specifically, MoS_2/WS_2 possessing a symmetric layered structure[5] and a corresponding bilayer nanotube.[25] (b) Structure of MLCs with alternate stacking of MX and TX_2 units[24] and single layer MLC nanotube.[26] (c) Layered structure of halloysite; the asymmetry between the Al-octahedra and Si-tetrahedra induces high strain forcing folding of the layer.[27−29] (d) Janus layer with broken inversion symmetry and MoSSe Janus nanotubes.[30] (e) Stability of the nanotube and nanostripes in comparison with bulk and monolayers. The energy/atom of the materials is reduced with an increasing number of layers stacked together. Note that under a critical size the nanoribbon becomes more stable than the nanotube (crossover point marked by pink arrows).[31] (f) Total energy of a nanotube calculated for various layered materials as a function of nanotube radius. Note that in contrast to the symmetric compounds, which are metastable (positive strain energy), the minimum in the energy diagram of imogolite signifies its absolute stability compared to the bulk flat structure.[32]

- Sreedhara, M. B.; Hettler, S.; Kaplan-Ashiri, I.; Rechav, K.; Feldman, Y.; Enyashin, A.; Houben, L.; Arenal, R.; Tenne, R. Asymmetric Misfit Nanotubes: Chemical Affinity Outwits the Entropy at High-temperature Solid-State Reactions. *Proc. Natl. Acad. Sci. U.S.A.* **2021**, *118* (35), e2109945118.[2] The study shows that even at elevated temperatures the Ln-based MLC system shows that chemical affinity plays a significant role over the entropy and leads to highly asymmetric nanotubes with broken inversion and time reversal symmetries.
- Hettler, S.; Sreedhara, M. B.; Serra, M.; Sinha, S. S.; Popovitz-Biro, R.; Pinkas, I.; Enyashin, A. N.; Tenne, R.; Arenal, R. YS-TaS_2 and $Y_xLa_{1-x}S$-TaS_2 ($0 \leq x \leq 1$) Nanotubes: A Family of Misfit Layered Compounds. *ACS Nano* **2020**, *14* (5), 5445−5458.[3] Explore the detailed structural analysis of misfit nanotubes and the effect of alloying on the yield, stability, and charge transfer characteristics of La(Y)S-TaS_2 MLC system.

INTRODUCTION

Materials with layered structures, like graphite and transition metal dichalcogenides (TMDCs), have attracted considerable interest in the scientific community for over a century.[4,5] These compounds are characterized by strong, mostly covalent, bonding between the atoms within the molecular slab (a–b plane). The molecular slabs are packed together (along the c-axis) via mostly weak van der Waals interlayer interactions. MoS_2 is one such layered structure material (see Figure 1a), which has been thoroughly investigated in recent years. Compounds with layered structure exhibit highly anisotropic physiochemical properties. One practical aspect of the anisotropy is that they can be easily cleaved in the a–b plane.[5] This practice allows revealing fresh surface suitable for many studies and more recently is a means to exfoliate the crystal and obtain a single layer of that compound. Among this group of anisotropic materials, the family of misfit layered compounds (MLCs) stands-out in its unique structure and physicochemical properties, which are not a simple combination of its binary building blocks. MLCs are incommensurate and nonstoichiometric materials made of periodic stacking of a layer with (distorted) rocksalt structure (MX abbreviated as O) alternately with hexagonal TX_2 (or T) layer (Figure 1b). MLC are schematically denoted as $(MX)_{1+y}(TX_2)_m$ (MX-TX_2 or O-T for brevity), where the parameter m denotes the number of TX_2 layers in the repeat unit. In MX-TX_2 MLCs

https://doi.org/10.1021/acs.accounts.4c00412
Acc. Chem. Res. 2024, 57, 3243−3253

where M = Sn, Pb, Rare earths; T = Sn, Nb, Ta, and X = S, Se, Te have a common *c*-axis for both subunits, but the $(a-b)$ plane of the two layers is incommensurate (usually along the *a*-axis).[6] In other words, the ratio between the unit cells of the *O* and *T* layers is irrational, which makes MLCs quasi-periodic compounds. The nonstoichiometric composition is expressed through the parameter $1 + y = 2a_T/a_O$ $(0.08 < y < 0.32)$.

The first misfit compound discussed in the literature was graphite intercalated $FeCl_3$.[7] Although typical MLC materials like $PbTiS_3$,[8] $PbNbS_3$,[9] $LnMX_3$[10] (Ln = rare earth, Bi; M = Ta, Nb, Ti, V; X = S, Se) were synthesized early on, the accurate assignment of their misfit structure was missing. The structure of MLC was revealed first by Kato et al., who studied $LaCrS_3$[11] and more generally by Makovicky and Hyde who also coined the term "misfit" compounds.[6,12−14] Sinusoidal height modulations studied with scanning probe microscopy are a manifestation of the built-in strain in the incommensurate MLC structure and a hallmark of its lattice relaxation mechanism.[15] More recently, systematic investigation of the structure of synthetic chalcogenide-based MLC came with the works of Wiegers,[16] Meerschaut and Rouxel,[17,18] and later on many others.[19,20]

MLCs have been investigated thoroughly over the years.[16−23] Figure 1b displays an ortho-pseudohexagonal unit of $(LaS)_{1.13}TaS_2$, along the *c*-direction with overall orthorhombic symmetry and the lattice parameters of TaS_2 (a, $b = \sqrt{3}\cdot a$).[24] In analogy to intercalation compounds, the stability of the MLC structure is augmented by charge transfer from the MX unit to the hexagonal TX_2. However, in contrast to typical intercalation compounds like Li_xCoO_2, where the degree of (Li) intercalation (x) is variable between zero to one, in the case of pristine MLC, this ratio is constant $(1+y)$. In the case of the rare-earth based LnS-TaS_2 series MLCs are particularly interesting, because most rare earth atoms prefer the +3 valency and hence the stability of these MLC compound is related to a charge transfer from the $5d$ (4f) level of the rare-earth atom to the partially filled $5d_{z^2}$ level of the tantalum atom. Owing to the hyperstoichiometry $(1 + y)$ of LnS with respect to TaS_2 in the MLC, a complete charge transfer from the Ln atom to Ta is not favorable and is partially compensated by defects, antisites, and other kinds of dislocations.

Recently, MLC chemistry received a twist and has been largely expanded by using out-of-equilibrium growth techniques, enabling metastable MLC structures. Most importantly among them is the modulated elemental reactants (MER) technique, which yields turbostratically misaligned MLCs (ferecrystals).[33,34] In another interesting work,[35] stable $(LaSe)_{1.14}NbSe_2$ and $(SmS)_{1.19}TaS_2$ and also metastable misfit structures, like the sequence $LaTa(Se_{0.5}S_{0.5})_3$, were prepared by mechanochemical reaction via ball milling and subsequent annealing at 1000 °C.

NANOTUBES

Pauling observed that layered alumino (magnesia)-silicates compounds can be categorized into two families—symmetric and asymmetric ones.[27] In the asymmetric compounds, see Figure 1c, such as halloysite $Al_2Si_2O_5(OH)_4{\cdot}2H_2O$) and chrysotile $(Mg_3(Si_2O_5)(OH)_4)$, the $(a-b)$ plane of the alumina (magnesia) octahedra is smaller than that of a pair of the interconnected silica tetrahedra. This asymmetry forces the entire layer to bend. It took another 20 years for such nanotubes to be visually confirmed once transmission electron microscopy (TEM) gained sufficient resolution.[28,29] A new class of asymmetric 2D-materials, the so-called *Janus* structures, are also notable. Owing to their asymmetric structures, Janus layered compounds are expected to form nanotubes (see Figure 1d). Indeed, Janus nanotubes have been investigated quite thoroughly via *ab initio* methods. For instance, the asymmetric Janus from the TMDCs or BiSI are subdued to a similar driving force for folding into nanotubes.[30] Such nanotubes exhibit an energy minimum in small diameter and could in principle be a stable phase at ambient conditions.[31,32] The first MoSSe nanotube synthesized on top of BN nanotube scaffold was recently reported.[36]

More than three decades ago, nanotubes from metal dichalcogenide compounds, like WS_2[25,37] (Figure 1a) and h-BN,[38,39] were reported opening a new chapter in the chemistry and nanotechnology of layered compounds. Unlike the mechanism proposed by Pauling,[27] here the driving force for nanotubes' formation requires surmounting of the large elastic energy of folding. The energy gained by healing the dangling bonds on the rim atoms of the slab more than compensates for the folding energy in the given size-range. Since the ratio between rim/bulk atoms increases upon shrinking the length of the slab, the nanotube becomes more stable than the flat 2D nanoflake (having the same number of atoms). This new so-called Kroto−Iijima−Tenne (KIT) mechanism has proven itself over and over again both experimentally and also via numerous *in-silico* calculations.[31,40,41] However, at a very small radius, the energetic penalty of folding the layer becomes excessively high, making the nanoribbon more stable than the nanotube. This crossover point (red arrow) is clearly shown in Figure 1e. Early *ab initio* calculations showed also[31,40] that the trilayer WS_2 (MoS_2) nanotubes gain extra stability by accommodating larger radii compared to carbon nanotubes (CNT) and also having more than one layer as seen in Figure 1e. Therefore, these multiwall nanotubes are stable over a limited range of diameters, e.g., 10−150 nm. Actually, this figure explains also the great difficulty to synthesize singlewall WS_2 (MoS_2) nanotubes, which is so common for CNT. Fundamentally, there is a great difference between the nanotubes obtained via the Pauling mechanism,[27,29,30] and those produced via the KIT mechanism.[22−25] While the nanotubes obtained from asymmetric layered compounds, like Janus[21] are stable, i.e., their strain energy goes through a minimum and is lower than the infinite layer, nanotubes derived from symmetric layered compounds, like CNT, BN, and WS_2, are metastable and their strain energy is always positive, as demonstrated in Figure 1f. In fact, the global stability of the asymmetric nanotubes could be the reason that imogolite and chrysotile nanotubes are stable on a geological time scale (billions of years) and are mined on the surface of the earth.

Presumably, the expedient combination of both the Pauling and the KIT mechanisms permitted successful synthesis of numerous MLC nanotubes (schematically presented in Figure 1b) in tangible amounts.[26] Figures 2a and S1 (in Supporting Information, SI) displays scanning electron microscopy image (SEM) of SmS-TaS_2 and LaS-TaS_2 nanotubes mixed with few MLC flakes of the same composition. Figure 2b shows a scanning transmission electron microscopy high-angle annular dark-field (STEM-HAADF) image of an individual nanotube and STEM energy dispersive X-ray spectroscopy (STEM-EDS) mapping of the different atoms making the MLC nanotube. The uniform distribution of the different atoms is testimony to the robustness of the nanotube synthesis. Figure 2c and d show

https://doi.org/10.1021/acs.accounts.4c00412
Acc. Chem. Res. 2024, 57, 3243−3253

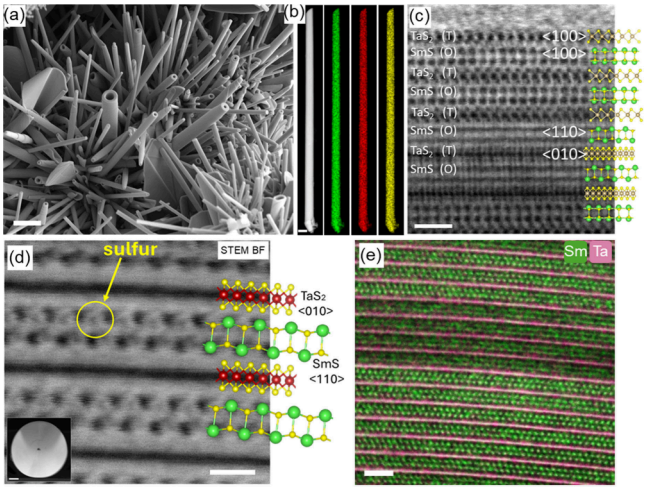

Figure 2. SEM image of SmS-TaS_2 nanotubes obtained by chemical vapor transport reaction at high temperatures using Cl as transport agent, scale bar 2 μm. (b) STEM-HAADF image of a single SmS-TaS_2 nanotube and the corresponding EDS chemical maps: Sm, green; Ta,red; and S, yellow; scale bar is 200 nm. (c) HR-STEM image of a nanotube showing the alternate stacking of rocksalt SmS and trigonal prismatic TaS_2 in the misfit lattice structure. Model structure and crystallographic orientations are overlaid on the STEM image. Scale bar: 1 nm. The contrast difference between first two and adjacent ones correspond to the $(O\text{-}T)(O\text{-}T)'$ hyperperiodicity. (d) Atomic resolution HR-STEM-BF image of a portion of the nanotube lamellae; a low magnification image of the cross-section shown in the inset, scale bar 100 nm. The magnified image reveals the sulfur atoms adjacent to samarium atoms in the rock salt unit, scale bar 1 nm. (e) Atomic resolution STEM-EDS chemical mapping of individual nanotube in cross-section geometry, Ta (red) and Sm (green) layers, scale bar 2 nm (Reproduced with modification from ref 42., copyright 2024, CC-BY 4.0, Authors).

high-resolution (HR)STEM bright-field (BF) images of a pristine nanotube in atomic resolution and a cross-section lamella prepared via focused ion beam (FIB) from one such nanotube. The lattice model of the MLC compound SmS-TaS_2 is overlaid on the HRSTEM image. Careful analysis of the atomic arrangement reveals tantalum and sulfur atoms coordinated in trigonal prismatic fashion in the TaS_2 layer and the SmS 100 plane in a distorted rocksalt configuration. The cross-section image in Figure 2d reveals the SmS 110 direction and the S atoms in the rock salt lattice. Figure 2e shows the atomically resolved chemical mapping obtained with STEM-EDS of the nanotube cross-section, revealing the alternating layers of samarium and tantalum.

More recently, the focus turned to MLC nanotubes consisting of four elements, especially alloying the rocksalt lattice and the anion sites (S/Se).[43] One remarkable property common to different MLC nanotubes is the hyperperiodicity of $(O\text{-}T)(O\text{-}T)'$ layers, whereby the $(O\text{-}T)'$ layer (armchair configuration) is titled 30° with respect to the adjacent $(O\text{-}T)$ layer (zigzag)—see Figures 2c and S2.[26,44,45] This hyperperiodicity is believed to be a manifestation of yet another strain relaxation mechanism in such nanotubes.

STOICHIOMETRY OF MLC NANOTUBES VS BULK MATERIAL

As stated above, the deviation from stoichiometry in MLC compounds is expressed through the term $1 + y = 2a_T/a_O$ ($0.08 < y < 0.32$). Figure S3 shows a schematic representation of an MLC bulk (a) and a nanotubular structure (b). For the case of nanotubes with $(O\text{-}T)$ periodicity, the stoichiometry is determined also via the respective diameter of each of the slabs (see schematics in Figure S3b). The TaS_2 makes always the outer layer and as is clearly seen in Figure S3b, if the circumference of the SmS wall is taken as $L_{SmS} = 2\pi R_{SmS}$ that of the TaS_2 layer is $- L_{TaS2} = 2\pi R_{TaS2} = 2\pi(R_{SmS} + d)$, where d is the spacing between the SmS and TaS_2 layers and $R_{O,T}$ is the radius of the O and T layers. Representing this feature in terms of stoichiometry, one could conclude that $1 + y_{NT}$ in $(SmS)_{1+y}TaS_2$ nanotube is smaller than in bulk $(SmS)_{1.19}TaS_2$ crystals. Therefore, for nanotubes one can write $1 + y_{NT} = (2a_T/a_O)/(L_{TaS2}/L_{SmS}) = 1.19/(1 + d/R_{SmS})$. Taking $d \sim 0.6$ nm and $R_{SmS} = 50$ nm, $1 + y_{NT} = 1.176$ instead of 1.19, i.e., 1.1% deviation from the overall bulk MLC stoichiometry. For an inner layer of the nanotube with $R_{SmS} = 10$ nm, the deviation from stoichiometry is $1 + y_{NT} = 1.122$, which represents a significant deviation (11%) from the bulk material. This deviation also means that the overall excess charge of the O layer in the nanotube is reduced with appreciably smaller charge transfer. Therefore, the Ta $5d_{z^2}$ level near the Fermi level is hole-rich (electron deficient) in the nanotube compared to the bulk MLC endowing the nanotube higher electrical conductivity than the bulk material. The actual deviation from stoichiometry $(1 + y_{NT})$ can be smaller since it can be partially compensated by defects, antisites, atom transfer from one layer to the other.

STABILITY OF NANOTUBES, GENERAL

The chemical selectivity and stability of MLC nanotubes versus their macroscopic flakes and also with respect to the binary compounds of their constituent atoms at low and mostly at elevated temperatures are discussed next. Another issue, which is not disconnected from the previous one, is the charge transfer from the MX slab to the TX_2 slab.

The chemical reactivity and high-temperature stability of fullerene-like (IF) nanoparticles of WS_2, MoS_2, and NbS_2 was investigated in inert and oxygenated atmospheres in comparison with the bulk crystallites.[46] It was found in an earlier study that the decomposition temperature of IF-WS_2 nanoparticles (containing also 10% nanotubes) was about 50 °C lower than that of the bulk material in inert atmosphere, i.e., 1250 vs 1300 °C for WS_2. However, a direct comparison with density functional theory (DFT) calculations of the high temperature behavior of inorganic nanotubes has not been done so far. Note, however, that phonon contributions to thermodynamic properties of different nanotubes as a function of temperature was estimated using zone folding approximation.[47]

CHEMICAL SELECTIVITY OF RARE-EARTH BASED MLC NANOTUBES

It is well-known in the literature that the distribution of sulfur and selenium in the TMDC lattice is random at elevated temperatures.[48,49] So far little has been done to elucidate the phase behavior of MLC at elevated temperatures,[50] let alone nanotubes thereof. While much effort has been invested over the last 30 years to perfect the synthetic routes of different (metastable) nanostructures, the question of their stability limits and decomposition pathways remains largely obscure. One major obstacle in this respect is the difficulty of comparing the experimental data to the *ab initio* calculations. Owing to the large unit cell of the "approximant" and the heavy

https://doi.org/10.1021/acs.accounts.4c00412
Acc. Chem. Res. 2024, 57, 3243−3253

atoms, *ab initio* calculations of MLC nanotubes are currently beyond reach. This also means that the simpler force-field analysis is of limited use under these circumstances because it cannot be parametrized against DFT calculations. Furthermore, *ab initio* calculations are generally limited to zero Kelvin (see, however, ref 51), and they are unable to address the high-temperature stability of nanotubes, accurately.

The stability and chemical selectivity of nanotubes belonging to the alloyed MLC La(S,Se)-$(Ta(S,Se)_2)_n$ was recently elucidated.[2] Surprisingly, the reaction of La, Ta, S and Se (up to 1100 °C) yielded MLC nanotubes with lanthanum atoms bonded exclusively to sulfur atoms and the selenium to tantalum atoms (as shown in Figure 3). Consequently, for x_{Se}<

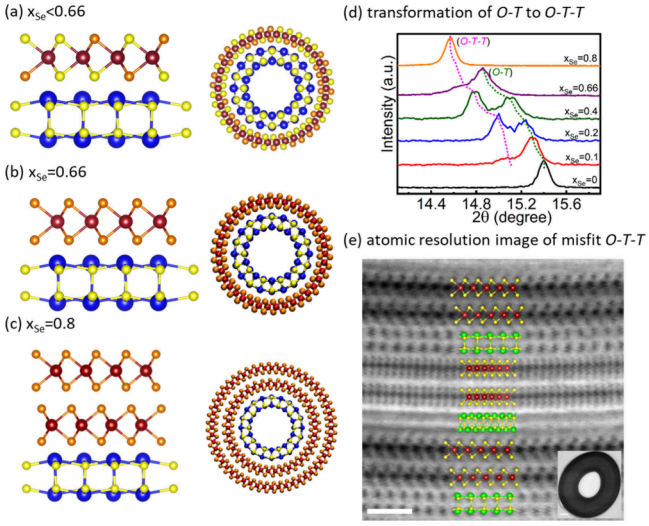

Figure 3. (a) Schematic rendering of the high temperature chemical affinity of MLC (*O-T*) layered structure with La exclusively binding to S (yellow) in the lattice and the corresponding nanotube geometry. (b) For x_{Se} = 0.66, notice the exclusive binding of Se (orange) with Ta and La with S. (c) Structure of MLC with (*O-T-T*) arrangement at the composition x_{Se} = 0.8 with selective binding Se with Ta and La with S. (d) Powder XRD pattern of LaS-TaS_2 with varying x_{Se} showing the gradual conversion of MLC (*O-T*) type lattice into (*O-T-T*) type lattice. (e) Atomic resolution HAADF-STEM image of nanotube cross-section lamella of the composition x_{Se} = 0.8 showing the (*O-T-T*) structure, a schematic model has been overlaid, scale bar 2 nm (Adapted from ref 2 with modifications, copyright 2024 Authors).

0.66, where $x_{Se} + x_s = 1$, the chemical composition of the nanotubes (and flakes) could be presented as LaS-$TaSe_{2x}S_{2(1-x)}$. At x_{Se} = 0.66 the amount of sulfur was sufficient to form nanotubes with the (*O-T*) formula LaS-$TaSe_2$. Upon increasing the *x*-value even further, partial starvation with respect to sulfur led to the formation of LaS-$TaSe_2$-$TaSe_2$ (*O-T-T*) nanotubes (and flakes). Figure 3b–c presents a schematic rendering of the nanotubes with (*O-T*) structure LaS-$TaSe_{2x}S_{2(1-x)}$ for $x < 0.66$; LaS-$TaSe_2$ for $0.66 < x < 0.8$ and LaS-$(TaSe_2)_2$ (*O-T-T*) for $x = 0.8$ and little beyond. In fact, the transitions are not abrupt, as can be visualized by the X-ray diffraction (XRD) patterns displayed in Figure 3d. Here the (*O-T-T*) peak is visible already for $x = 0.2$, but the (*O-T*) peak is diminished entirely for $x = 0.8$, indicating smooth transition from (*O-T*) to (*O-T-T*) structure due to the gradual starvation with respect to sulfur. Figure 3e shows a high-resolution STEM (HRSTEM) image of a lamella cut from an (*O-T-T*) nanotube prepared from sample with x = 0.8. Not only the (*O-T-T*) structure is confirmed, but also the hyperperiodicity, i.e., LaS-$(TaSe_2)_2$, LaS-$(TaSe_2)_2'$ structure with 30° tilt between the two adjacent (*O-T-T*) pairs is validated.

Ultimately, when the sulfur content was limited further, the MLC nanotubes (and flakes) became unstable and no MLC nanotubes (or flakes) based on pure selenium, i.e., LaSe-$TaSe_2$ could be found. To understand this surprising chemical selectivity, one should bear in mind that the stability of MLC is enabled by the charge transfer from the LaS to $TaSe_2$.[52] Once an MLC superstructure (*O-T-T-T*) is formed, the middle $TaSe_2$ does not contact any LaS layer, preventing efficient charge transfer and leading to a reduced stability of the superstructure. In this case, the MLC was found to decompose into $TaSe_2$, pure selenium, and some binary lanthanum chalcogenide compound. Here too, the hyperperiodicity of the form (*O-T*)(*O-T*)′ and (*O-T-T*)(*O-T-T*)′ with 30° inclination of the (*O-T*)′ layer with respect to the adjacent (*O-T*) one was common in the nanotubes. The conspicuous chemical selectivity of the lanthanum atom toward sulfur and the selenium atom toward tantalum at elevated temperatures was recently found to go beyond lanthanum and encompasses other rare earth atoms.

In the present perspective, the stabilities of $(LaS)_{1.14}TaS_2$ and $(SmS)_{1.19}TaS_2$ nanotubes are studied as a function of the synthesis time and temperatures. A preliminary study on this topic was recently published,[1] and is largely expanded by including synchrotron-based X-ray absorption (XAS) and diffraction anomalous fine structure (DAFS) techniques. This expansion allows for a more profound understanding of the decomposition process of the MLC nanotubes at elevated temperatures.

THE THERMAL STABILITY OF MLC NANOTUBES AT ELEVATED TEMPERATURES STUDIED BY SYNCHROTRON-BASED X-RAY TECHNIQUES

Recently, the thermal stability of SmS-TaS_2 and LaS-TaS_2 nanotubes were investigated.[1] In the first series of experiments (Table S1), the nanotubes were synthesized at different temperatures (from 800 to 975 °C). In the second series of experiments, the materials were synthesized at the optimal temperature (825 and 875 °C for the Sm- and La-based nanotubes, respectively) for different time-intervals. In the third kind of experiment, the MLC nanotubes were prepared in quartz ampules at their optimal condition, i.e., 825 and 875 °C for 4 h for the Sm- and La-based MLC nanotubes (Figures 2a and S1, respectively. The as-synthesized nanotubes went through an annealing process above 1000 °C (see Table S1 for the description). The laboratory based XRD patterns for both temperature and time series of SmS-TaS_2[1] and LaS-TaS_2 (Figures S4 and S5) MLCs show highly preferred (00*l*) orientation and also indicate the gradual structural transformation from (*O-T*) to (*O-T-T*) and then to (*O-T-T-T*). The preferred orientation overshadows the (*0kl*) reflections, making it difficult to analyze the conversion of nanotubes into flakes.

Diffraction patterns of the nanotubes mainly consist of the sharp 00*l* reflections that are associated with the interlayer spacing and the *hk*0 reflections that are heavily streaked due to translation stacking disorder associated with the direction perpendicular to nanotube axis (Figure S2).[53−60] Due to the lack of the out-of-plane symmetry of the curved nanostructures

https://doi.org/10.1021/acs.accounts.4c00412
Acc. Chem. Res. 2024, 57, 3243−3253

and circumferential disorder between layers, the diffraction patterns of the nanotubes do not exhibit the distinct and sharp *hkl* reflections (with $l \neq 0$, namely *h0l* and *0kl*) that distinguish them from the bulk particles—see Table 1. These diffraction

Table 1. Reflection Conditions for the Most Common Phases in the Powder Containing Bulk, Single-Layer 2D Materials, and Their Nanotubes[b]

Reflections	Bulk particles/Multilayered flakes (platelets)	Nanotubes	Single layers
00*l*	+	+	–
*hk*0	+	+	+
*h*0*l*	+	–[a]	–
0*kl*	+	–[a]	–

Adopted from reference 1, copyright 2024, CC-BY 4.0, Authors. [a]This peak is not absolutely forbidden for large diameter tubes, where the curvature is small. [b]The *h*0*l* and 0*kl* reflections will be absent for nanotubes.

features first observed in carbon nanotubes using electron microscopy were also observed in MLC nanotubes with the help of synchrotron-based subμm XRD.[1] Spatially dispersing the SmS-TaS_2 nanotubes and SmS-TaS_2 flakes on the SiN grid away from each other, it was possible to get the XRD patterns from single MLC nanotubes and flakes, thus revealing their differences—see Figure S6. Generally, while the 00*l* peaks belong to both the nanotubes and flakes, the 0*kl* peaks can be assigned solely to the flakes. These results provide the tools for analyzing the temperature and time dependence of the nanotubes, summarized in the next series of experiments described below.

In the following experiments, the products were analyzed via electron microscopy, X-ray powder diffraction, synchrotron-based X-ray diffraction, X-ray absorption spectroscopy (XAS), and diffraction anomalous fine-structure (DAFS).

The synchrotron-based XRD analysis of SmS-TaS_2 and LaS-TaS_2 as a function of the synthesis temperature is discussed in the SI and shown in Figures S7 and S8, respectively. This analysis shows clearly that the abundance of the nanotubes goes down with temperature. It also shows a gradual transformation from the (*O*-*T*) superstructure to the (*O*-*T*-*T*) superstructure, with the La-based MLC being more prone to this transformation. Above 1100 °C a third process, i.e., decomposition of the MLC phases into binary sulfides and partial oxidation are observed. These transformations are also discussed further below.

EFFECT OF THE SYNTHESIS TEMPERATURE STUDIED VIA X-RAY ABSORPTION SPECTROSCOPY (XAS) AND DIFFRACTION ANOMALOUS FINE-STRUCTURE (DAFS) MEASUREMENTS

XAS spectra measured in the transmission mode of the SmS-TaS_2 samples (absorption) for the temperature series in the vicinity of the Ta L_3 edge are presented in Figure 4. From the extended X-ray absorption fine structure (EXAFS) region (Figure 4b) it is seen that there is no significant change in the oscillation amplitudes with the temperature of the synthesis, indicating that the local structure of the tantalum atom (bond distance, etc.) remains almost the same. The white line of the XAS spectrum at X-ray absorption near edge (XANES) region is due to electron excitation from the occupied 2*p* core level of

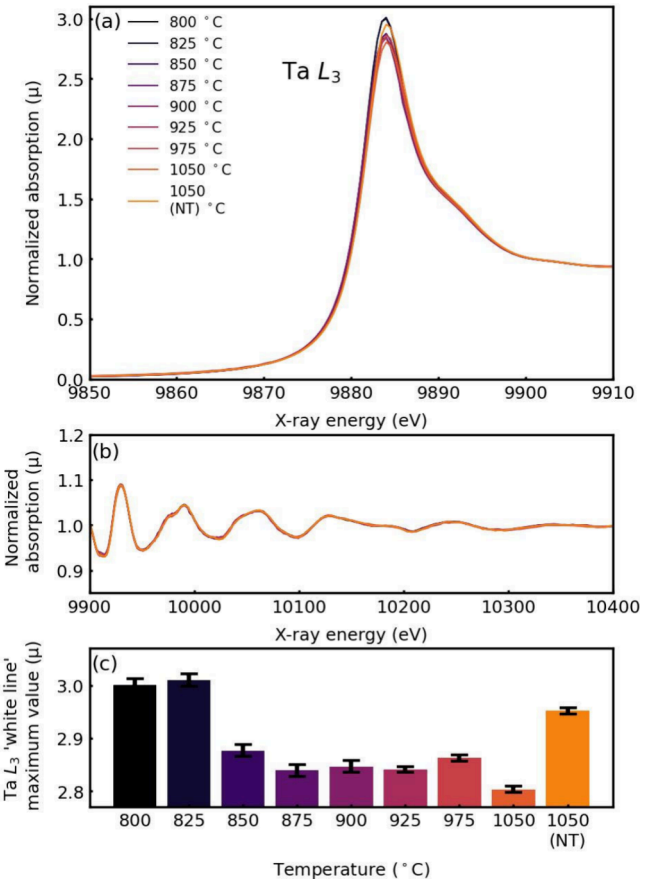

Figure 4. X-ray absorption spectra in the vicinity of the Ta L_3 edge of SmS-TaS_2 samples achieved at different temperatures: XANES (a) and EXAFS (b) regions. The (c) shows the height of the Ta L_3 white line as a function of temperature.

tantalum into its empty $5d_{z^2}$ state near the Fermi level. It is noticed that the Ta L_3 white line intensity decreases with increasing temperature (Figure 4c). One can see a strong step change at 850 °C, and then a plateau at the temperature range 850–975 °C. Then at 1050 °C the intensity falls again. The drop in the intensity of the white line can be attributed to the filling of the Ta $5d_{z^2}$ state with electrons, which is indicative of the nanotubes-to-flakes transformation with temperature, as well as (*O*-*T*) to (*O*-*T*-*T*) transformation and decomposition of the MLC into binary TaS_2. These transformations are discussed in connection with the XRD analysis (Figures S7 and S8) in the SI text. The block 1050 (NT) summarizes the results of an experiment in which the product was prepared at 825 °C (>50% nanotubes abundancy) and subsequently annealed at 1050 °C for 4 h. Remarkably, the high intensity of the white line after 1050 °C annealing indicates that the decomposition of the nanotubes is retarded, compared to the direct synthesis of the product at temperatures above 850 °C. One plausible explanation is that the chlorine gas, which drives the CVT reaction and consequently also the phase transformation, has been frozen-out during the intermediate cooling of the ampule to room temperature between the synthesis (at 825 °C) and the annealing 1050 °C. Another plausible explanation is that the reaction product has decomposed into binary TaS_2 and other byproducts, like $Sm_2Ta_3S_2O_8$ upon annealing.[48] Being richer in free carriers (holes), pure TaS_2

https://doi.org/10.1021/acs.accounts.4c00412
Acc. Chem. Res. 2024, 57, 3243–3253

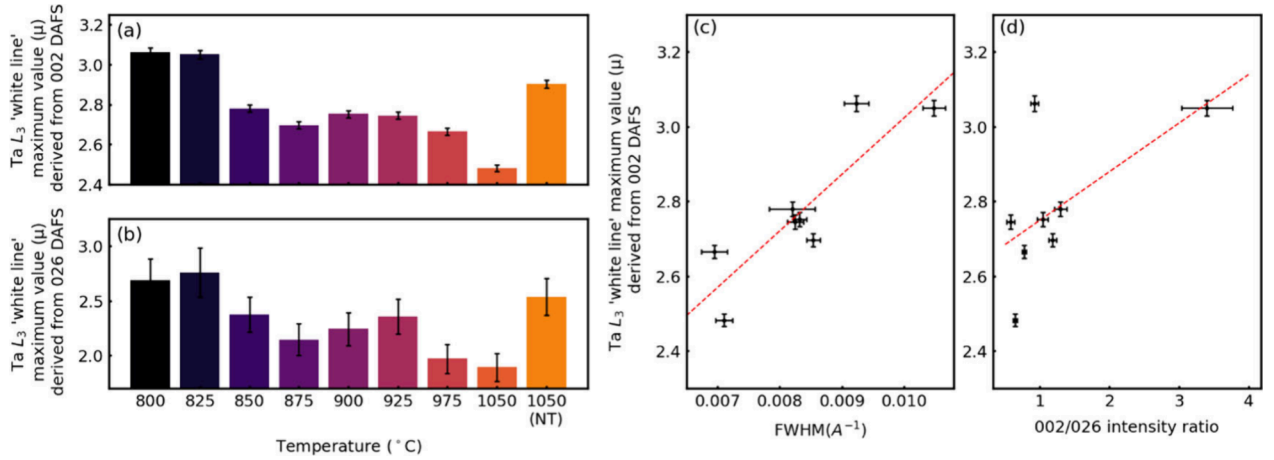

Figure 5. White line intensities derived from the 002 (a) and 026 (b) DAFS reflections of SmS-TaS_2 as a function of temperature; (c) and (d) represents the white line intensity of the 002 reflection on the fwhm and nanotube abundance (002/026), correspondingly.

would lead to a stronger white line compared with the MLC. This point is discussed further below.

However, it is necessary to analyze the DAFS data in order to clean the nanotube XAS signal from the influence of other phases present in the samples. The DAFS technique is based on measurements of the diffraction peak intensity in the vicinity of the X-ray absorption edge.[61−65] Contrary to conventional XAS,[66,67] DAFS allows measuring the XAS-like signal from certain phase or crystallographic site separately by choosing the proper diffraction peak, thus providing phase- and site-selectivity. Thus, by choosing the diffraction peak from a certain phase within the powder mixture, one will get spectroscopic information solely from this phase from DAFS measurement. In the present DAFS analysis logarithmic dispersion relation (LDR) approach proposed by Kawaguchi[64,65] was used. Detailed description of the DAFS experimental setup (Figure S9), as well as the procedure for data analysis can be found in the Supporting Information.

According to the discussion above (and Table 1), one can use the 026 reflection for getting the spectroscopic information from the MLC flakes and the 002 reflection for receiving the information from both tubes and platelets with the DAFS method. An example of the DAFS experimental data for SmS-TaS_2 is presented in Figure S10, where the variation of the diffraction intensity of these reflections in the vicinity of the Ta L_3 edge is clearly visible. Figure S11 presents the DAFS (reflection) spectrum of the 002 and 026 diffraction peaks intensity of SmS-TaS_2 samples at different temperatures, and Figure 5 represents its analysis. Figure 5a and b shows block diagrams of the white line (DAFS) intensity derived from the 002 and 026 reflections as a function of temperature, correspondingly. The intensity of the 026 reflection is appreciably weaker in comparison to the 002 peak and also overlaps partially with the 0010 peak (Figure 5b). Therefore, the measured intensity of this reflection has a large error bar. Here too, the white line is due to electron excitation of the occupied $2p$ core level of tantalum into its empty $5d_z^2$ state near the Fermi level. The reduced intensity of the 002 reflection white line of SmS-TaS_2 upon increasing the temperature (Figure 5a) suggests that the Ta $5d_z^2$ level is being filled with electrons and the free carrier (holes) density goes down with increasing growth temperature. This finding is compatible with the transformation of the substoichiometric nanotubes into MLC flakes, which incorporates extra electron-rich samarium (in the $4f^6$ level). It is also compatible with the transformation of the (*O*-*T*) phase into (*O*-*T*-*T*), where the charge transferred from the SmS (*O*) is shared between two TaS_2 (*T*) layers, as seen in the 1050-nanotube sample. Remarkably, the intensities of the "white" line of the sample annealed at 1050 °C after being synthesized at 825 °C (1050 (NT)) are high indicating that the nanotubes are not easily transformed into flakes in this process. Alternatively (or conjointly), it may indicate that the nanotubes have been decomposed into TaS_2 and other side-products.

However, as shown in the lower panel of Figure 5b, the intensity of the white line associated with the 026, which belongs exclusively to the MLC flakes, goes down as well with the temperature. To explain this phenomenon, one must evoke another mechanism which could contribute to the white line intensity i.e., the surface density of the tantalum atoms. One such explanation for the weakening of the white line of the 026 DAFS peak with temperature is related to the effect of the surface atoms. It has been established in the past[68] that surface effects play an important part in the white line intensity for nanoparticles. The intensity of the white line of the Pt surface atoms was larger in comparison to atoms in the bulk. Therefore, the white line from both MLC flakes and nanotubes should, in principle, depend on the particle size because the influence of the surface atoms becomes significant at small particle sizes. In addition, notwithstanding the large error bars, Figure 5c and d demonstrate that the white line intensity (straight line is a guide to the eye) increases with the abundancy of the nanotubes as manifested via the FWHM (Figure 5c) and the 002/026 intensity ratio. Therefore, the transformation of the nanotubes into large flakes at higher temperatures leads to a reduced white line intensity, which is ascribed, among others, to a smaller surface density of tantalum atoms in the flakes compared with the nanotubes. Again, the increased intensity of the white line of the 1050 (NT) can be putatively ascribed to transformation of the MLC into binary TaS_2 and other byproducts. Here, the explanation of the white line intensity behavior is of qualitative character and partially based on XRD observations; quantitative considerations require XAS computer simulations based on nanotube structural models, which are beyond the focus of this perspective.

https://doi.org/10.1021/acs.accounts.4c00412
Acc. Chem. Res. 2024, 57, 3243−3253

EFFECT OF THE SYNTHESIS TIME

Figure S12 in SI summarizes the results of the annealing time (1 to 90 h) of the LaS-TaS_2 MLC with synchrotron-based XRD. First, the obvious nanotubes-to-flakes transformation with annealing time is clearly observed. Most outstandingly, however, a clear transformation of the (*O-T*) structure into (*O-T-T*) after 8 h synthesis and subsequent transformation of the (*O-T-T*) into (*O-T-T-T*) phase after 16 h synthesis time is omnipresent. This autocatalytic transformation is not exclusive to this system and is common in intercalation chemistry including Li-ion batteries.[69,70]

Figure 6 presents the X-ray absorption near the Ta L_3 edge for LaS-TaS_2 as a function of the reaction time. In analogy to the case of SmS-TaS_2, the EXAFS region (Figure 6b) shows no significant change of the oscillation amplitudes with heating time, indicating that the local structure (bond distance, type, and number of neighbors) remains almost unchanged with annealing time. The block diagram in Figure 6c shows that the intensity of the white line increases slightly after 2 h and then gradually decreases up to 8 h, which suggests that the charge transfer from the LaS slab to the TaS_2 slab goes down with annealing time, for reasons explained above for the temperature series of the SmS-TaS_2 MLC (transformation of the MLC tubes into flakes). However, a sharp rise in the intensity of the white line occurs after 16 h followed by a small decline in its intensity after 90 h annealing time. This significant intensity variation of the white line is indicative of a major transformation in the La-based MLC after 16 h. In particular, this intensity rise is attributed to a significant deintercalation of the LaS layer from the (*O-T*) lattice periodicity to form a new (*O-T-T*) and sequentially to (*O-T-T-T*) periodicity as seen on the XRD data (Figures S5 and S12b and c). The transformation of (*O-T-T*) to (*O-T-T-T*) periodicity is further confirmed by HAADF-STEM imaging (Figure S13). Furthermore, the high temperature transformation of the MLC phase into binary TaS_2 and LaS_x and other byproducts could also make an important contribution to this variation in intensity variation.

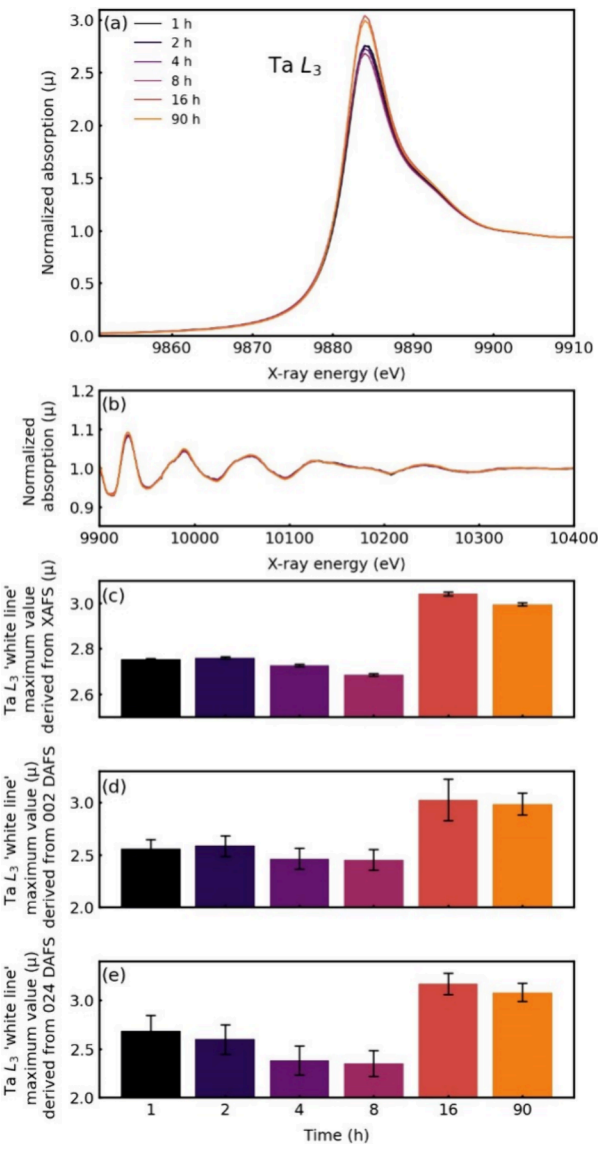

Figure 6. X-ray absorption spectra in the vicinity of the Ta L_3 edge of LaS-TaS_2 samples obtained at 875 °C with varying reaction time: XANES (a) and EXAFS (b) regions. (c) shows the height of the Ta L_3 white line as a function of reaction time; white line intensities of the DAFS spectra derived from the 002 (d) and 024 (e) peaks as a function of time.

All these processes imply that the LaS → TaS_2 charge transfer is greatly reduced and hence the free hole concentration of the $5d_{z^2}$ level of Ta increases sharply with the synthesis time. The same trend is observed in the block diagram of Figure 6d and 6e, which presents the strength of the white lines obtained from 002 and 024 DAFS, correspondingly (see also Figure S14). The similarity between the independent XAS data (Figure 6c) and the DAFS data (Figure 6d and e) is not accidental, offering a similar interpretation.

CONCLUSIONS AND OUTLOOK

Like most other nanophases, nanotubes formed from inorganic compounds based on a layer structure are metastable and are converted to macroscopic crystallites upon prolonged heating. This view is validated also in the case of nanotubes from misfit layer compounds (MLC), which are the topic of the present perspective. Using electron microscopy and mostly synchrotron-based X-ray reflection and absorption techniques (XRD, XAS, and DAFS), the mechanisms of such transformations were investigated in hitherto unknown detail. First, the chemical selectivity of the constituent metal atoms of the MLC nanotubes toward the chalcogen atom is examined. Notwithstanding the high temperature of the synthesis (up to 1000 °C), sulfur atoms are shown to bind exclusively to the rare-earth atom of the rocksalt slab, while selenium binds solely to the tantalum of the hexagonal TX_2 slab. This surprising selectivity is attributed to the large enthalpy of formation of the MLC nanotubes. Using selection rules for the XRD and diffraction anomalous fine-structure (DAFS) reflections of nanotubes as well as X-ray absorption (XAS), the common transformation of sulfide-based rear earth MLC nanotubes into microscopic flakes is investigated. The conspicuous transformation of (*O-T*) nanotubes (and flakes) into (*O-T-T*) and sequentially (*O-T-T-T*) phases at elevated temperatures is investigated. This autocatalytic reaction is in fact a reminiscent of the electrocatalytic deintercalation of lithium from the anode material in Li-ion batteries. Furthermore, partial oxidation of the product at elevated temperature was observed and discussed. Annealing at higher temperatures (>1100 °C) and for longer periods of time (up to 90 h) leads eventually to

https://doi.org/10.1021/acs.accounts.4c00412
Acc. Chem. Res. 2024, 57, 3243−3253

the decomposition of the ternary MLC into binary metal-sulfide phases.

While no immediate application for MLC nanotubes is visible in the near future, they may offer intriguing observations and potential exploitation in the future as anode materials for intercalation batteries,[71] electrocatalysis, for electronics,[72] thermoelectrics,[73] and in quantum technologies.[74] Their catalytic and electrocatalytic properties are yet another aspect to be explored. Their limited stability under an oxidative environment limits their uses under cathodic conditions, like hydrogen evolution reaction, or for CO_2 sequestration.

■ ASSOCIATED CONTENT

Supporting Information

The Supporting Information is available free of charge at https://pubs.acs.org/doi/10.1021/acs.accounts.4c00412.

Sample description for LaS-TaS_2 (Table S1), electron microscopy images, XRD of time and temperature series LaS-TaS_2 series, synchrotron experiments description of single nanotube diffraction, and description and analysis of XAS and DAFS spectral features (PDF)

■ AUTHOR INFORMATION

Corresponding Authors

M. B. Sreedhara − *Solid State and Structural Chemistry Unit, Indian Institute of Science, Bengaluru 560012, India;* orcid.org/0000-0003-4925-4346; Email: sreedhara@iisc.ac.in

Reshef Tenne − *Department of Molecular Chemistry and Materials Science, Weizmann Institute of Science, Rehovot 7610001, Israel;* orcid.org/0000-0003-4071-0325; Email: reshef.tenne@weizmann.ac.il

Authors

Azat Khadiev − *Deutsches Elektronen-Synchrotron DESY, 22607 Hamburg, Germany*

Simon Hettler − *Instituto de Nanociencia y Materiales de Aragon (INMA), CSIC-Universidad de Zaragoza, 50018 Zaragoza, Spain; Laboratorio de Microscopias Avanzadas (LMA), Universidad de Zaragoza, 50018 Zaragoza, Spain;* orcid.org/0000-0002-9102-7895

Dmitri Novikov − *Deutsches Elektronen-Synchrotron DESY, 22607 Hamburg, Germany*

Raul Arenal − *Instituto de Nanociencia y Materiales de Aragon (INMA), CSIC-Universidad de Zaragoza, 50018 Zaragoza, Spain; Laboratorio de Microscopias Avanzadas (LMA), Universidad de Zaragoza, 50018 Zaragoza, Spain; ARAID Foundation, 50018 Zaragoza, Spain;* orcid.org/0000-0002-2071-9093

Complete contact information is available at: https://pubs.acs.org/10.1021/acs.accounts.4c00412

Author Contributions

†A.K. and M.B.S. contributed equally

Notes

The authors declare no competing financial interest.

Biographies

Azat Khadiev received his Ph.D. from the Kazan National Research Technical University in 2016 (Russia). In 2018, he joined the "In-situ X-ray Diffraction and Imaging Beamline" at the PETRA III synchrotron at DESY (Germany) as a postdoctoral researcher and is now working there as a staff scientist. His main research interests are in the application of modern synchrotron X-ray techniques for studies of nano and functional materials.

M. B. Sreedhara obtained his Ph.D in Material Science from Jawaharlal Nehru Centre for Advanced Scientific Research (JNCASR), Bangalore, India (2018). He worked as a postdoctoral fellow in JNCASR (2018-2019) and in the Department of Materials and Interfaces at the Weizmann Institute of Science, Rehovot, Israel (2019-2023). He is currently an Assistant Professor at the Solid State and Structural Chemistry Unit, Indian Institute of Science (IISc), Bengaluru, India. His research focuses on the growth, design, and discovery of new hybrid and functional nanoscale and quantum materials for faster, cleaner and sustainable energy technologies.

Dmitri Novikov received his Ph.D. in solid state physics from the Institute of Crystallography of the USSR Academy of Sciences in 1988. He is currently a scientist in charge of the In-situ X-ray Diffraction and Imaging Beamline at the PETRA III synchrotron at DESY, Germany. His research interests focus on applied research and the development of new methods for X-ray analysis.

Simon Hettler received his PhD in Physics from the Karlsruhe Institute for Technology (Germany) in 2015 and is currently at the Instituto de Nanociencia y Materiales de Aragón at CSIC-Universidad de Zaragoza (Spain). His main research interests are the application of transmission electron microscopy and related spectroscopies on nanomaterials and a methodological development of microscopic techniques, recently focusing on *in situ* investigations.

Raul Arenal received his Ph.D. in 2005 in Solid State Physics from Paris XI Univ. (France) and obtained his HDR in 2013 also at this University. In 2007, he became research scientist at the CNRS (France). Since 2012, he is on leave from the CNRS and he is currently ARAID senior research scientist at the Instituto de Nanociencia y Materiales de Aragon (INMA) at CSIC-Universidad de Zaragoza (Spain). His broad area of research interest lies in electron microscopy focused on nanoscience: TEM (HR(S)TEM, electron diffraction, EELS, electron tomography, in situ). These studies are mainly focused on the growth mechanism and structural and physical properties of materials based on carbon and related nanomaterials as well as other nanostructures.

Reshef Tenne was born in 1944 in Kibbutz Usha, Israel. He earned his Ph.D. in 1976 in the Hebrew University. He joined the Weizmann Institute in 1979, where he was promoted to a professor in 1995. In 1992, he discovered a new family of nanomaterials—the so-called inorganic nanotubes (INT) and fullerene-like (IF) nanoparticles from layered compounds (2D materials). He and his research group synthesized and studied many kinds of inorganic nanotubes. He received numerous prizes and is a member of the Israeli Academy of Sciences and Humanities, Academia Europaea, and the European Academy of Arts and Sciences.

■ ACKNOWLEDGMENTS

We acknowledge DESY (Hamburg, Germany), a member of the Helmholtz Association HGF, for the provision of experimental facilities. Parts of this research were carried out at DESY P23 "In-situ X-ray diffraction and imaging beamline". Beamtime was allocated for proposal H-20010090 and I-20210786 EC. The authors thank Wolfgang Calibe and Aleksandr Kalinko from DESY P64 beamline for providing the Lambda Si detector and Yves Joly for the useful discussion on XAS and DAFS. M.B.S. acknowledges the Indian Institute of Science for the support and start-up grant funding. R.T.

acknowledges the support of The Estate of Manfred Hecht and the Estate of Diane Recanati. We are also grateful to the Irving and Cherna Moskowitz Center for Nano and Bio-Nano Imaging, the Perlman Family Foundation, and the Kimmel Center for Nanoscale Science. R.A. and S.H. acknowledge funding from the European Union's Horizon 2020 research innovation programme under the Marie Sklodowska-Curie grant agreement No 889546, by the Gobierno de Aragón (DGA) under project E13-23R, as well as by the Spanish Ministry of Science, Innovation and Universities (MICIU) (PID2019-104739GB-100/AEI/10.13039/501100011033) and by the 'Severo Ochoa' Programme for Centres of Excellence in R&D of the Spanish MICIU (CEX2023-001286-S MICIU/AEI/10.13039/501100011033).

REFERENCES

(1) Sreedhara, M. B.; Khadiev, A.; Zheng, K.; Hettler, S.; Serra, M.; Castelli, I. E.; Arenal, R.; Novikov, D.; Tenne, R. Nanotubes from Lanthanide-Based Misfit-Layered Compounds: Understanding the Growth, Thermodynamic, and Kinetic Stability Limits. *Chem. Mater.* **2024**, *36* (9), 4736−4749.

(2) Sreedhara, M. B.; Hettler, S.; Kaplan-Ashiri, I.; Rechav, K.; Feldman, Y.; Enyashin, A.; Houben, L.; Arenal, R.; Tenne, R. Asymmetric misfit nanotubes: Chemical affinity outwits the entropy at high-temperature solid-state reactions. *Proc. Natl. Acad. Sci. U.S.A.* **2021**, *118* (35), No. e2109945118.

(3) Hettler, S.; Sreedhara, M. B.; Serra, M.; Sinha, S. S.; Popovitz-Biro, R.; Pinkas, I.; Enyashin, A. N.; Tenne, R.; Arenal, R. YS-TaS_2 and $Y_xLa_{1-x}S$-TaS_2 ($0 \leq x \leq 1$) Nanotubes: A Family of Misfit Layered Compounds. *ACS Nano* **2020**, *14* (5), 5445−5458.

(4) Bernal, J. D.; Bragg, W. L. The structure of graphite. *Proc. R. Soc. A* **1924**, *106* (740), 749−773.

(5) Dickinson, R. G.; Pauling, L. The crystal structure of molybdenite. *J. Am. Chem. Soc.* **1923**, *45* (6), 1466−1471.

(6) Wiegers, G. A.; Meetsma, A.; van Smaalen, S.; Haange, R. J.; Wulff, J.; Zeinstra, T.; de Boer, J. L.; Kuypers, S.; Van Tendeloo, G.; Van Landuyt, J.; et al. Misfit layer compounds (MS)nTS_2 (M = Sn, Pb, Bi, rare earth elements; T = Nb, Ta; n = 1.08 - 1.19), a new class of layer compounds. *Solid State Commun.* **1989**, *70* (4), 409−413.

(7) Cowley, J. M.; Ibers, J. A. The structures of some ferric chloride-graphite compounds. *Acta Crystallogr.* **1956**, *9* (5), 421−431.

(8) Sterzel, W. Darstellung und Eigenschaften von Bleithiotitanat. *Naturwissenschaften* **1966**, *53* (8), 199−199.

(9) Schmidt, L. Superconductivity in $PbNbS_3$ and $PbTaS_3$. *Phys. Lett. A* **1970**, *31* (10), 551−552.

(10) Donohue, P. C. Preparation and properties of $LnMX_3$, where Ln = rare earths, Bi; M = Ta, Nb, Ti, V, and X = S, Se. *J. Solid State Chem.* **1975**, *12* (1), 80−83.

(11) Kato, K.; Kawada, I.; Takahashi, T. Die Kristallstruktur von $LaCrS_3$. *Acta Cryst. B* **1977**, *33* (11), 3437−3443.

(12) Makovicky, E.; Hyde, B. G. Non-commensurate (misfit) layer structures. In *Inorganic Chemistry; Structure and Bonding*, Inorganic Chemistry, Vol. *46*; Springer: Berlin, 1981; pp 101−170.

(13) Makovicky, E.; Hyde, B. Incommensurate, two-layer structures with complex crystal chemistry: minerals and related synthetics. In *Materials Science Forum*; Trans Tech Publ., 1992; Vol. *100*, pp 1−100.

(14) Makovicky, E. Crystal Structures of Complex Lanthanide Sulfides With Built-in Non-Commensurability. *Aust. J. Chem.* **1992**, *45* (9), 1451−1472.

(15) Henriksen, R. B.; Makovicky, E.; Stipp, S. L. S.; Nissen, C.; Eggleston, C. M. Atomic-scale observations of franckeite surface morphology. *Am. Mineral.* **2002**, *87* (10), 1273−1278.

(16) Wiegers, G. A.; Meetsma, A.; Haange, R. J.; de Boer, J. L. Structure and physical properties of $(SnS)_{1.18}NbS_2$, "$SnNbS_3$", a compound with misfit layer structure. *Mater. Res. Bull.* **1988**, *23* (11), 1551−1559.

(17) Guemas, L.; Rabu, P.; Meerschaut, A.; Rouxel, J. Characterization of new "$SnNbS_3$, $PbNbS_3$, $PbNb_2S_5$, $SnTiS_3$ and $SnTi_2S_5$" compounds. *Mater. Res. Bull.* **1988**, *23* (7), 1061−1069.

(18) Guemas, L.; Rabu, P.; Meerschaut, A.; Rouxel, J. Characterization of new "$SnNbS_3$, $PbNbS_3$, $PbNb_2S_5$, $SnTiS_3$ and $SnTi_2S_5$" compounds. *Mater. Res. Bull.* **1988**, *23* (7), 1061−1069.

(19) Gotoh, Y.; Goto, M.; Kawaguchi, K.; Oosawa, Y.; Onoda, M. Preparation and characterization of a new composite-layered sulfide, $(PbS)_{1.12}VS_2$, "$PbVS_3$. *Mater. Res. Bull.* **1990**, *25* (3), 307−314.

(20) Ohno, Y. Electronic structure of the misfit-layer compounds $PbTiS_3$ and $SnNbS_3$. *Phys. Rev. B* **1991**, *44* (3), 1281−1291.

(21) Meerschaut, A. Misfit layer compounds. *Current Opinion in Solid State and Materials Sci.* **1996**, *1* (2), 250−259.

(22) Wiegers, G. A. Misfit layer compounds: Structures and physical properties. *Prog. Solid State Chem.* **1996**, *24* (1), 1−139.

(23) Ng, N.; McQueen, T. M. Misfit layered compounds: Unique, tunable heterostructured materials with untapped properties. *APL Mater.* **2022**, *10* (10), 100901.

(24) Wiegers, G. A.; Meetsma, A.; Haange, R. J.; de Boer, J. L. Structure, electrical transport and magnetic properties of the misfit layer compound $(SmS)_{1.19}TaS_2$ "$SmTaS_3$. *J. Less Common Met.* **1991**, *168* (2), 347−359.

(25) Tenne, R.; Margulis, L.; Genut, M.; Hodes, G. Polyhedral and cylindrical structures of tungsten disulphide. *Nature* **1992**, *360* (6403), 444−446.

(26) Panchakarla, L. S.; Radovsky, G.; Houben, L.; Popovitz-Biro, R.; Dunin-Borkowski, R. E.; Tenne, R. Nanotubes from Misfit Layered Compounds: A New Family of Materials with Low Dimensionality. *J. Phys. Chem. Lett.* **2014**, *5* (21), 3724−3736.

(27) Pauling, L. The Structure of the Chlorites. *Proc. Natl. Acad. Sci. U.S.A.* **1930**, *16* (9), 578−582.

(28) Turkevich, J.; Hillier, J. Electron Microscopy of Colloidal Systems. *Anal. Chem.* **1949**, *21* (4), 475−485.

(29) Bates, T. F.; Sand, L. B.; Mink, J. F. Tubular Crystals of Chrysotile Asbestos. *Science* **1950**, *111* (2889), 512.

(30) Zheng, K.; Vegge, T.; Castelli, I. E. Giant In-Plane Flexoelectricity and Radial Polarization in Janus IV-VI Monolayers and Nanotubes. *ACS Appl. Mater. Interfaces* **2024**, *16* (15), 19369−19378.

(31) Enyashin, A.; Gemming, S.; Seifert, G. Nanosized allotropes of molybdenum disulfide. *Eur. Phys. J. Spec. Top.* **2007**, *149* (1), 103−125.

(32) Enyashin, A.; Seifert, G. In *Handbook of Nanophysics: Nanotubes and Nanowires*, 1st ed.; Sattler, K. D. E., Ed.; CRC Press, 2010. DOI: 10.1201/9781420075434.

(33) Westover, R. D.; Ditto, J.; Falmbigl, M.; Hay, Z. L.; Johnson, D. C. Synthesis and Characterization of Quaternary Monolayer Thick $MoSe_2$/SnSe/$NbSe_2$/SnSe Heterojunction Superlattices. *Chem. Mater.* **2015**, *27* (18), 6411−6417.

(34) Choffel, M. A.; Kam, T. M.; Johnson, D. C. Substituent Effects in the Synthesis of Heterostructures. *Inorg. Chem.* **2021**, *60* (13), 9598−9606.

(35) Dolotko, O.; Hlova, I. Z.; Pathak, A. K.; Mudryk, Y.; Pecharsky, V. K.; Singh, P.; Johnson, D. D.; Boote, B. W.; Li, J.; Smith, E. A.; et al. Unprecedented generation of 3D heterostructures by mechanochemical disassembly and re-ordering of incommensurate metal chalcogenides. *Nat. Commun.* **2020**, *11* (1), 3005.

(36) Yang, C.; Lin, Q.; Sato, Y.; Gao, Y.; Zheng, Y.; Wang, T.; Ma, Y.; Maruyama, M.; Okada, S.; Suenaga, K. Janus MoSSe nanotubes on one-dimensional SWCNT-BNNT van der Waals heterostructures. *arXiv* **2024**, No. 2407.15145.

(37) Feldman, Y.; Wasserman, E.; Srolovitz, D. J.; Tenne, R. High-Rate, Gas-Phase Growth of MoS_2 Nested Inorganic Fullerenes and Nanotubes. *Science* **1995**, *267* (5195), 222−225.

(38) Rubio, A.; Corkill, J. L.; Cohen, M. L. Theory of graphitic boron nitride nanotubes. *Phys. Rev. B* **1994**, *49* (7), 5081−5084.

(39) Chopra, N. G.; Luyken, R. J.; Cherrey, K.; Crespi, V. H.; Cohen, M. L.; Louie, S. G.; Zettl, A. Boron Nitride Nanotubes. *Science* **1995**, *269* (5226), 966−967.

https://doi.org/10.1021/acs.accounts.4c00412
Acc. Chem. Res. 2024, 57, 3243−3253

(40) Enyashin, A.; Gemming, S.; Seifert, G. *Springer Ser. Mater. Sci.* **2007**, *93*, 33−59.
(41) Evarestov, R. A. *Theoretical Modeling of Inorganic Nanostructures: Symmetry and Ab-Initio Calculations of Nanolayers, Nanotubes and Nanowires*; Springer, 2015.
(42) Sreedhara, M. B.; Bukvisova, K.; Khadiev, A.; Citterberg, D.; Cohen, H.; Balema, V.; K. Pathak, A.; Novikov, D.; Leitus, G.; Kaplan-Ashiri, I.; Kolibal, M.; Enyashin, A. N.; Houben, L.; Tenne, R. Tenne, Nanotubes from the Misfit Layered Compound $(SmS)_{1.19}TaS_2$: Atomic Structure, Charge-Transfer and Electrical Properties. *Chem. Mater.* **2022**, *34*, 1838.
(43) Aliev, S. B.; Tenne, R. Quaternary Misfit Compounds—A Concise Review. *Crystals* **2020**, *10* (6), 468.
(44) Lorenz, T.; Joswig, J.-O.; Seifert, G. Two-dimensional and tubular structures of misfit compounds: Structural and electronic properties. *Beilstein J. Nanotechnol.* **2014**, *5*, 2171−2178.
(45) Radovsky, G.; Popovitz-Biro, R.; Tenne, R. Nanotubes from the Misfit Layered Compounds MS-TaS_2, Where M = Pb, Sn, Sb, or Bi: Synthesis and Study of Their Structure. *Chem. Mater.* **2014**, *26* (12), 3757−3770.
(46) Schuffenhauer, C.; Wildermuth, G.; Felsche, J.; Tenne, R. How stable are inorganic fullerene-like particles? Thermal analysis (STA) of inorganic fullerene-like NbS_2, MoS_2, and WS_2 in oxidizing and inert atmospheres in comparison with the bulk material. *Phys. Chem. Chem. Phys.* **2004**, *6* (15), 3991−4002.
(47) Bandura, A. V.; Porsev, V. V.; Evarestov, R. A. Application of zone-folding approach to the first-principles estimation of thermodynamic properties of carbon and ZrS2-based nanotubes. *J. Comput. Chem.* **2016**, *37* (7), 641−652.
(48) Sreedhara, M. B.; Miroshnikov, Y.; Zheng, K.; Houben, L.; Hettler, S.; Arenal, R.; Pinkas, I.; Sinha, S. S.; Castelli, I. E.; Tenne, R. Nanotubes from Ternary $WS_{2(1-x)}Se_{2x}$ Alloys: Stoichiometry Modulated Tunable Optical Properties. *J. Am. Chem. Soc.* **2022**, *144* (23), 10530−10542.
(49) Albert L. Sino, P.; Lin, T.-C.; Wani, S.; Lee, L.; Chen, C.-T.; Liu, M.-J.; Kuo, Y.-Z.; Rehman, B.; Tuyen Le, K.; Wu, J.-M.; Chuang, F.-C.; Chueh, Y.-L.; et al. Controllable structure-engineered janus and alloy polymorphic monolayer transition metal dichalcogenides by plasma-assisted selenization process toward high-yield and wafer-scale production. *Mater. Today* **2023**, *69*, 97−106.
(50) Reisinger, G. R.; Richter, K. W. The 550 and 700 °C isothermal sections and new misfit layer compounds in the Se-Sn-V system. *J. Alloys Compd.* **2021**, *871*, 159573.
(51) Duff, A. I.; Davey, T.; Korbmacher, D.; Glensk, A.; Grabowski, B.; Neugebauer, J.; Finnis, M. W. Improved method of calculating ab initio high-temperature thermodynamic properties with application to ZrC. *Phys. Rev. B* **2015**, *91* (21), 214311.
(52) Lorenz, T.; Baburin, I. A.; Joswig, J.-O.; Seifert, G. Charge Transfer Variability in Misfit Layer Compounds: Comparison of SnS-SnS_2 and LaS-TaS_2. *Isr. J. Chem.* **2017**, *57* (6), 553−559.
(53) Amelinckx, S.; Devouard, B.; Baronnet, A. Geometrical Aspects of the Diffraction Space of Serpentine Rolled Microstructures: their Study by means of Electron Diffraction and Microscopy. *Acta Crystallogr.* **1996**, *52* (6), 850−878.
(54) Zhang, X. B.; Zhang, X. F.; Amelinckx, S.; Van Tendeloo, G.; Van Landuyt, J. The reciprocal space of carbon tubes: a detailed interpretation of the electron diffraction effects. *Ultramicroscopy* **1994**, *54* (2), 237−249.
(55) Dódony, I. Structure of the 30-sectored polygonal serpentine. A model based on TEM and SAED studies. *Phys. Chem. Min* **1997**, *24* (1), 39−49.
(56) Lambin, P.; Lucas, a. Quantitative theory of diffraction by carbon nanotubes. *Phys. Rev. B* **1997**, *56* (7), 3571−3574.
(57) Khalitov, Z.; Khadiev, A.; Pashin, D. Electron diffraction patterns from scroll nanotubes: interpretation peculiarities. *J. Appl. Crystallogr.* **2015**, *48* (1), 29−36.
(58) Khalitov, Z.; Khadiev, A.; Valeeva, D.; Pashin, D. Structure of ordered coaxial and scroll nanotubes: general approach. *Acta Crystallogr. Sect. A Found. Adv.* **2016**, *72* (1), 36−49.
(59) Khalitov, Z.; Khadiev, A.; Valeeva, D.; Pashin, D. Quantitative theory of diffraction by ordered coaxial nanotubes: reciprocal-lattice and diffraction pattern indexing. *Acta Crystallogr. Sect. A Found. Adv.* **2016**, *72* (6), 684−695.
(60) Khadiev, A.; Khalitov, Z. Quantitative theory of diffraction by cylindrical scroll nanotubes. *Acta Crystallographica Section A Foundations and Advances* **2018**, *74* (3), 233−244.
(61) Stragier, H.; Cross, J.; Rehr, J.; Sorensen, L. B.; Bouldin, C.; Woicik, J. Diffraction anomalous fine structure: A new x-ray structural technique. *Phys. Rev. Lett.* **1992**, *69* (21), 3064.
(62) Pickering, I. J.; Sansone, M.; Marsch, J.; George, G. N. Diffraction anomalous fine structure: a new technique for probing local atomic environment. *J. Am. Chem. Soc.* **1993**, *115* (14), 6302−6311.
(63) Vacinova, J.; Hodeau, J.; Wolfers, P.; Lauriat, J.; ElKaim, E. Use of anomalous diffraction, DAFS and DANES techniques for site-selective spectroscopy of complex oxides. *J. Synchrotron Radiat.* **1995**, *2* (5), 236−244.
(64) Kawaguchi, T.; Fukuda, K.; Tokuda, K.; Shimada, K.; Ichitsubo, T.; Oishi, M.; Mizuki, J.; Matsubara, E. Revisit to diffraction anomalous fine structure. *J. Synchrotron Radiat.* **2014**, *21* (6), 1247−1251.
(65) Kawaguchi, T.; Fukuda, K.; Matsubara, E. Site- and phase-selective x-ray absorption spectroscopy based on phase-retrieval calculation. *J. Phys.: Condens. Matter* **2017**, *29* (11), 113002.
(66) Koningsberger, D. C.; Mojet, B. L.; van Dorssen, G. E.; Ramaker, D. E. XAFS spectroscopy; fundamental principles and data analysis. *Top. Catal.* **2000**, *10* (3), 143−155.
(67) Gaur, A.; Shrivastava, B. D.; Nigam, H. X-ray absorption fine structure (XAFS) spectroscopy-a review. *Proc. Indian Natl. Sci. Acad.* **2013**, *79*, 921−966.
(68) Bazin, D.; Sayers, D.; Rehr, J. J.; Mottet, C. Numerical Simulation of the Platinum LIII Edge White Line Relative to Nanometer Scale Clusters. *J. Phys. Chem. B* **1997**, *101* (27), 5332−5336.
(69) Charalambous, H.; Borkiewicz, O. J.; Colclasure, A. M.; Yang, Z.; Dunlop, A. R.; Trask, S. E.; Jansen, A. N.; Bloom, I. D.; Ruett, U.; Wiaderek, K. M.; et al. Comprehensive Insights into Nucleation, Autocatalytic Growth, and Stripping Efficiency for Lithium Plating in Full Cells. *ACS Energy Lett.* **2021**, *6* (10), 3725−3733.
(70) MacNeil, D. D.; Christensen, L.; Landucci, J.; Paulsen, J. M.; Dahn, J. R. An Autocatalytic Mechanism for the Reaction of Li_x CoO_2 in Electrolyte at Elevated Temperature. *J. Electrochem. Soc.* **2000**, *147* (3), 970.
(71) Huang, Y.-E.; Lin, W.; Shi, C.; Li, L.; Fan, K.; Huang, X.-Y.; Wu, X.; Du, K.-Z. Misfit layer $SnTiS_3$: An assemble-free van der Waals heterostructure SnS/TiS_2 for lithium ion battery anode. *J. Power Sources* **2021**, *494*, 229712.
(72) Zullo, L.; Marini, G.; Cren, T.; Calandra, M. Misfit Layer Compounds as Ultratunable Field Effect Transistors: From Charge Transfer Control to Emergent Superconductivity. *Nano Lett.* **2023**, *23* (14), 6658−6663.
(73) Taneja, V.; Goyal, N.; Das, S.; Chandra, S.; Dutta, P.; Ravishankar, N.; Biswas, K. Nanostructured Ferecrystal Intergrowths with $TaSe_2$ Unveiled High Thermoelectric Performance in n-Type SnSe. *J. Am. Chem. Soc.* **2024**, *146*, 24716.
(74) Leriche, R. T.; Palacio-Morales, A.; Campetella, M.; Tresca, C.; Sasaki, S.; Brun, C.; Debontridder, F.; David, P.; Arfaoui, I.; Šofranko, O.; et al. Misfit Layer Compounds: A Platform for Heavily Doped 2D Transition Metal Dichalcogenides. *Adv. Funct. Mater.* **2021**, *31* (6), 2007706.

https://doi.org/10.1021/acs.accounts.4c00412
Acc. Chem. Res. 2024, 57, 3243−3253